Boron-doped NiCoP Nanoarrays with Wrinkle Grown on Carbon Cloth for Hybrid Supercapacitor Application

Zhe Zhang[a], Xuetao Zhang[b], Chunqing Tai[a], Mingzhi Wei[*, a, c], Qifang Lu[a], Enyan Guo[a], Conghui Si[a], Shunwei Chen[a], Xiujun Han[a]

[a]Shandong Provincial Key Laboratory of Processing and Testing Technology of Glass & Functional Ceramics, School of Material Science and Engineering, Qilu University of Technology (Shandong Academy of Sciences), Jinan 250353, China

[b]Beijing Key Laboratory of Microstructure and Properties of Solids, Faculty of Materials and Manufacturing, Beijing University of Technology, Beijing 100124, China

[c]De zhou Institute of Qilu University of Technology (Shandong Academy of Sciences), Dezhou, China

*Corresponding authors.

E-mail: weimz2018@163.com

Chemicals

Sinopharm Chemical Reagent Co. Ltd. was the supplier of chemicals, which were used as purchased. The syntheses of the NiCoP and B-NiCoP samples were prepared by carbon cloth, Nitric acid (GR), acetone (AR), ($Ni(NO_3)_2 \cdot 6H_2O$, 99.9%), ($Co(NO_3)_2 \cdot 6H_2O$, 99.9%), urea (99%), $NaH_2PO_2 \cdot H_2O$ (95%), $NaBH_4$, KOH, deionized water (DI) and ethanol. The activated carbon used was purchased from Fuzhou, China, model: YEC-8.

Materials characterization

The crystalline structur was pointed out by a powder X-ray diffraction (XRD, Bruker, AXS D8) with Cu Kα (λ = 0.15406 nm). The morphologies were demonstrated by scanning electron microscopy (SEM, JEOL JSM-6700F) and transmission electron microscope (TEM, JEOL JEM-2010). Surface element composition and chemical state analysis of the sample were characterized by XPS (ESCALABXi+).

Electrochemical test of supercapacitor

To further evaluate the electrochemical performance of NCP, B-NCP-16, B-NCP-18, and B-NCP-20, the cyclic voltammetry (CV), galvanostatic charge-discharge test (GCD), and electrochemical impedance spectroscopy (EIS) were performed using a CHI760E electrochemical workstation. The platinum sheet and Hg/HgO electrode were used as counter electrodes and reference electrodes, respectively, and 3 M KOH aqueous solution was used as electrolyte.

The specific capacity of NCP, B-NCP-16, B-NCP-18, and B-NCP-20 was calculated using the following equation:

$$C = (I \times \Delta t)/m \tag{1}$$

while the specific capacitance of AC was calculated using the following equation:

$$C = (I \times \Delta t)/(m \times \Delta V) \tag{2}$$

where I (A) is the discharge current, ΔV (V) is the width of the potential window, Δt (s) is the time of discharge, and m (g) is the loading mass of active material.

For the two-electrode system, B-NCP-18 was used as the positive electrode, activated carbon as the negative electrode and 3 M KOH as the electrolyte to assemble

B-NCP-18‖AC hybrid supercapacitors. The area of the active material was 1×2 cm^2. The mass loadings of AC were controlled based on the balanced charge principle.

$$C_+ \times m_+ \times (\Delta V)_+ = C_- \times m_- \times (\Delta V)_- \tag{3}$$

where m_+/m_- is the mass of anode/cathode material. The mass loadings of AC were 9.64 mg.

The energy density (E, Wh kg^{-1}), and power densities (P, W kg^{-1}) of HSCs were calculated according to the following equations:

$$C = (I \times \Delta t)/m \tag{4}$$

$$E = (\int IU(t)dt)/3.6m \tag{5}$$

$$P = (3600 \times E)/\Delta t \tag{6}$$

where C (C g^{-1}) refers to the specific capacity, I (A) is the discharge current, Δt (s) is the time of discharge, m (g) is the loading mass of active material, and U (V) is the width of the potential window.

Computational details

All calculations were based on DFT, executed by Vienna Ab-initio Simulation Package (VASP). The whole three-dimensional (3D) periodic models were constructed by Materials Studio (MS). The Perdew-Burke-Ernzerhof (PBE) of generalized gradient approximation (GGA) was used to describe the exchange-correlation effect. The core interactions were treated using the pseudo-potential of projector-augmented-wave (PAW) method. In this study, the NiCoP model was obtained by subjecting the NiCoP protocells to a 2×2 supercell. The energy cutoff of 520 eV and $3 \times 3 \times 10$ k-points for entire geometry calculation. The Hubbard-U correction was adopted for better description of the localized d-electrons of Ni and Co in their hydroxides. We chose an effective U−J value of 6.4 eV and 3.3 eV for Ni and Co atoms, respectively. All the geometry structures and atomic positions were fully relaxed by a conjugate gradient (CG) method with convergence criteria of 0.02 eV Å^{-1} and 10^{-5} eV atom^{-1} for force and energy, respectively.

The following formula has been used to calculate the E$_{ads}$:

$$E_{ads} = E_{slab+adsorbent} - E_{slab} - E_{adsorbent}$$

where E_{slab}, $E_{adsorbent}$, and $E_{slab+adsorbent}$ are the total energies of the optimized slab of structures, adsorbents, and slab+adsorbent systems, respectively.
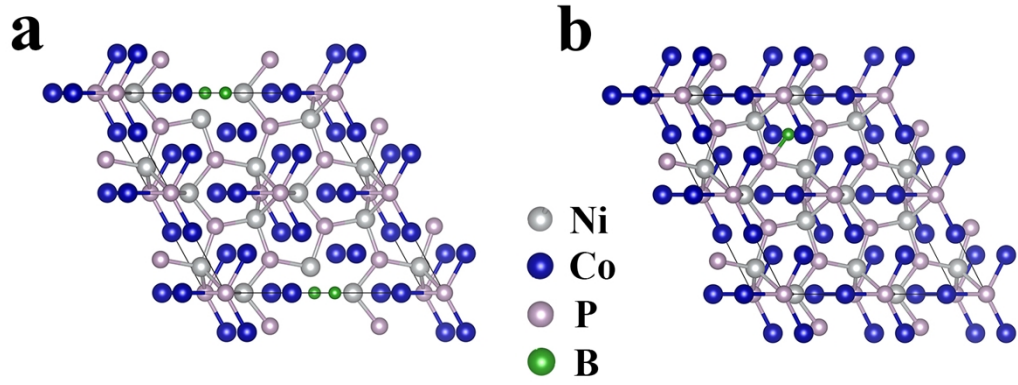
Fig. S1 The optimization model for substitutional doping and interstitial doping of B doped NiCoP
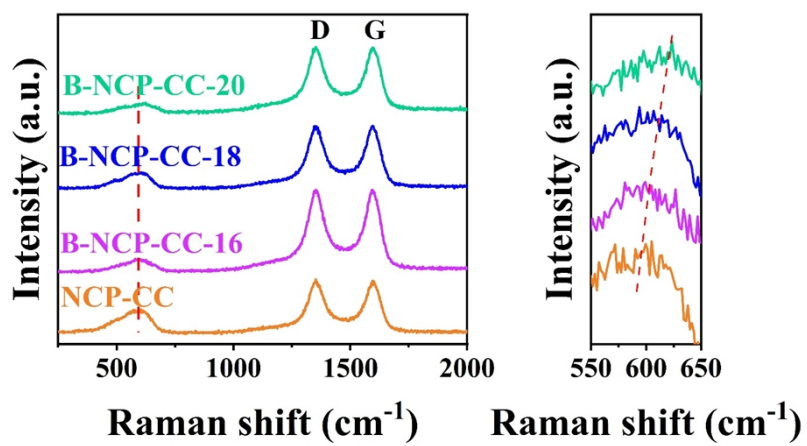
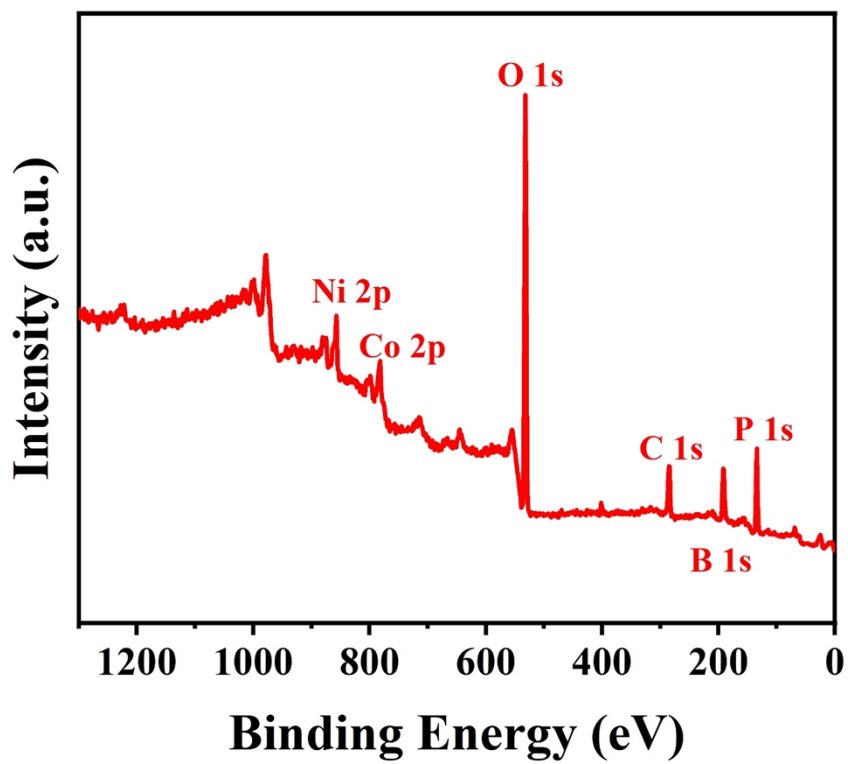**Fig. S2** Raman spectra of NCP-CC, B-NCP-CC-16, B-NCP-CC-18, and B-NCP-CC-20
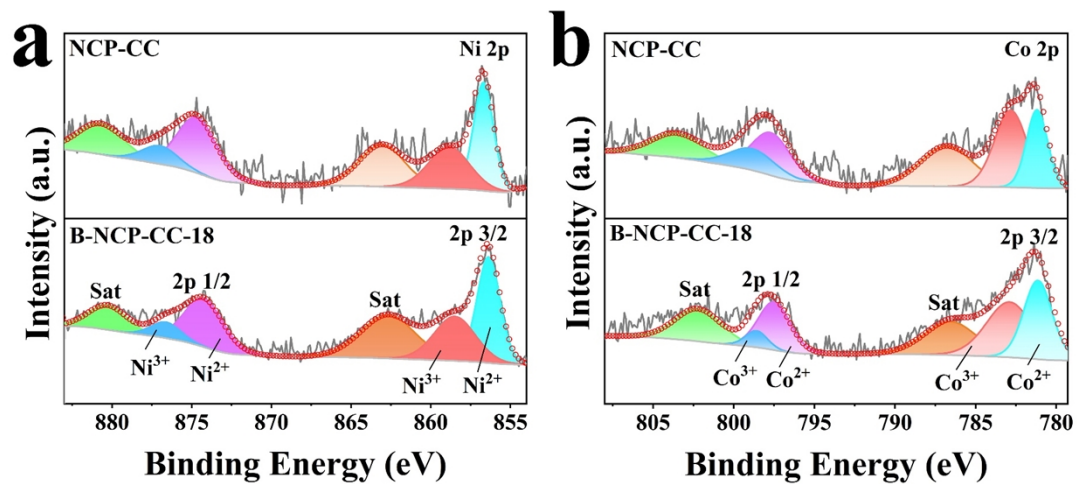
Fig. S3 XPS survey spectrum of B-NCP-CC-18

Fig. S4 Comparison of high-resolution XPS spectra of NCP-CC and B-NCP-CC-18 (a) Ni 2p, (b) Co 2p
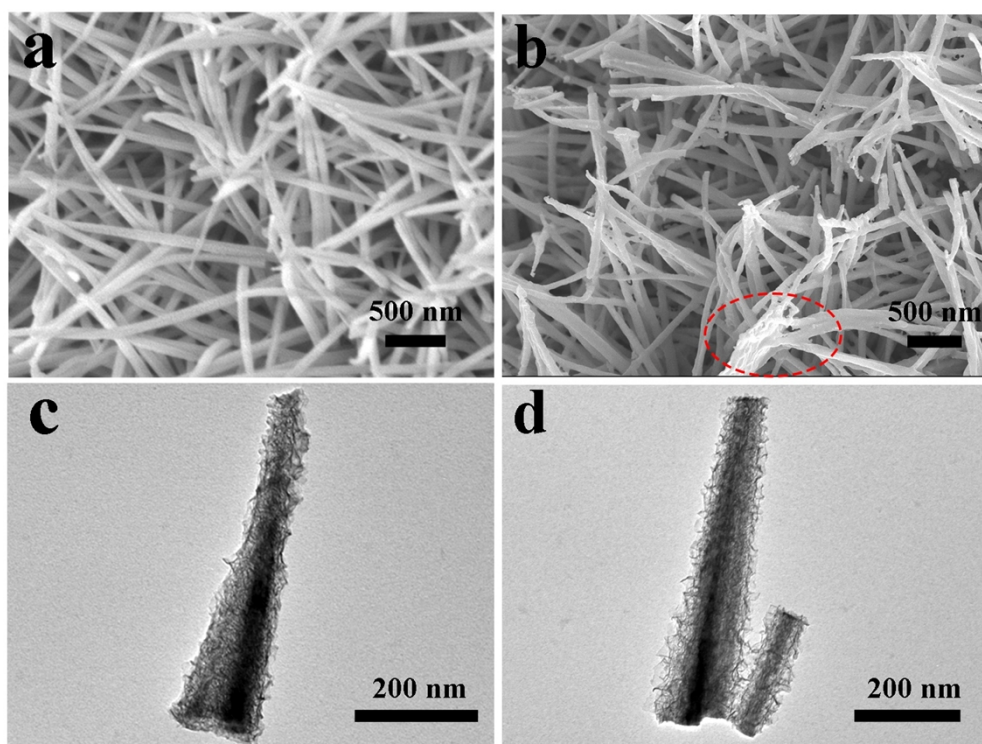
Fig. S5 SEM images of (a)B-NCP-CC-16 and (b)B-NCP-CC-20; and TEM images of (c)B-NCP-CC-16 and (d)B-NCP-CC-20.
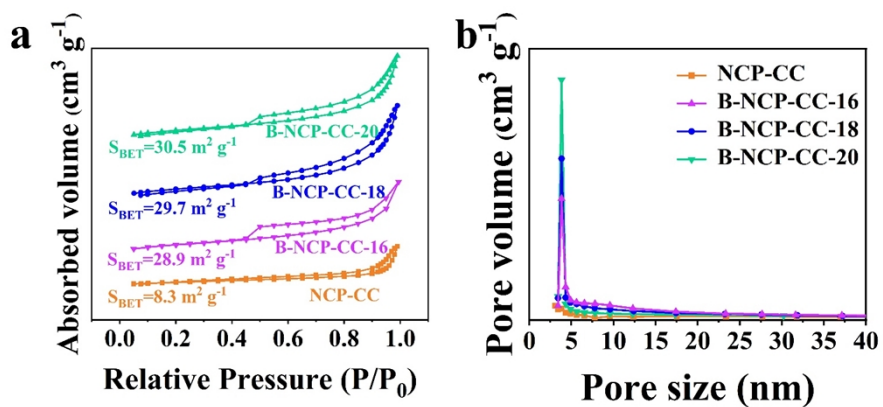
Fig. S6 (a) N_2 absorption/desorption isotherms and (b) pore size distributions of NCP-CC, B-NCP-CC-16, B-NCP-CC-18, and B-NCP-CC-20.
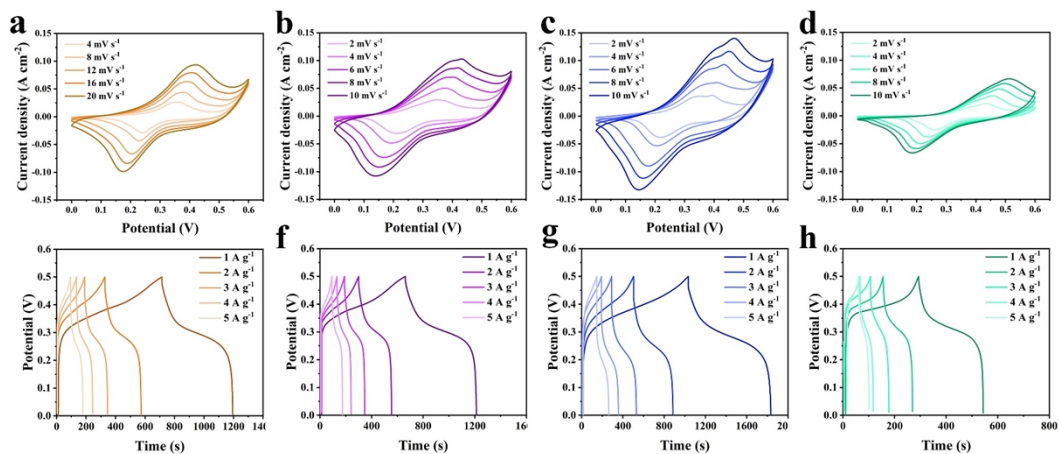
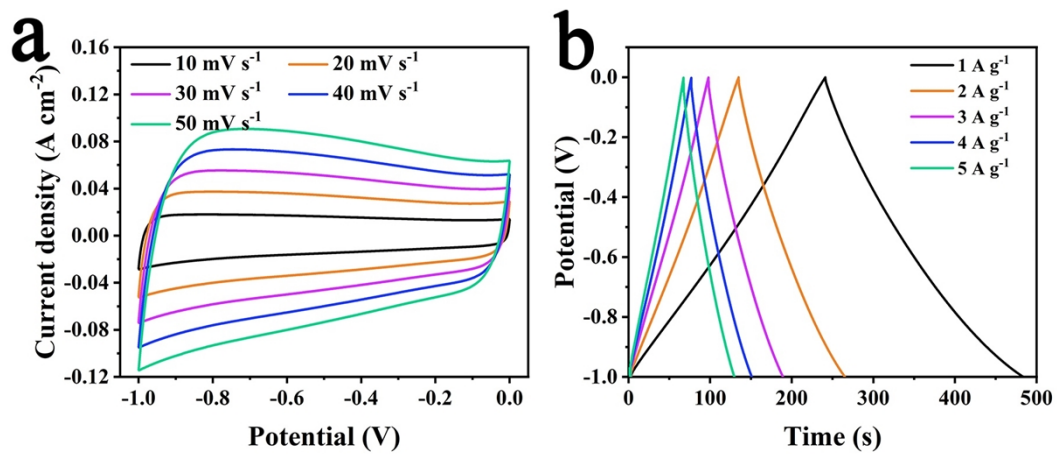**Fig. S7** (a-d) CV curves and (e-h) GCD curves of NCP-CC, B-NCP-CC-16, B-NCP-CC-18, and B-NCP-CC-20
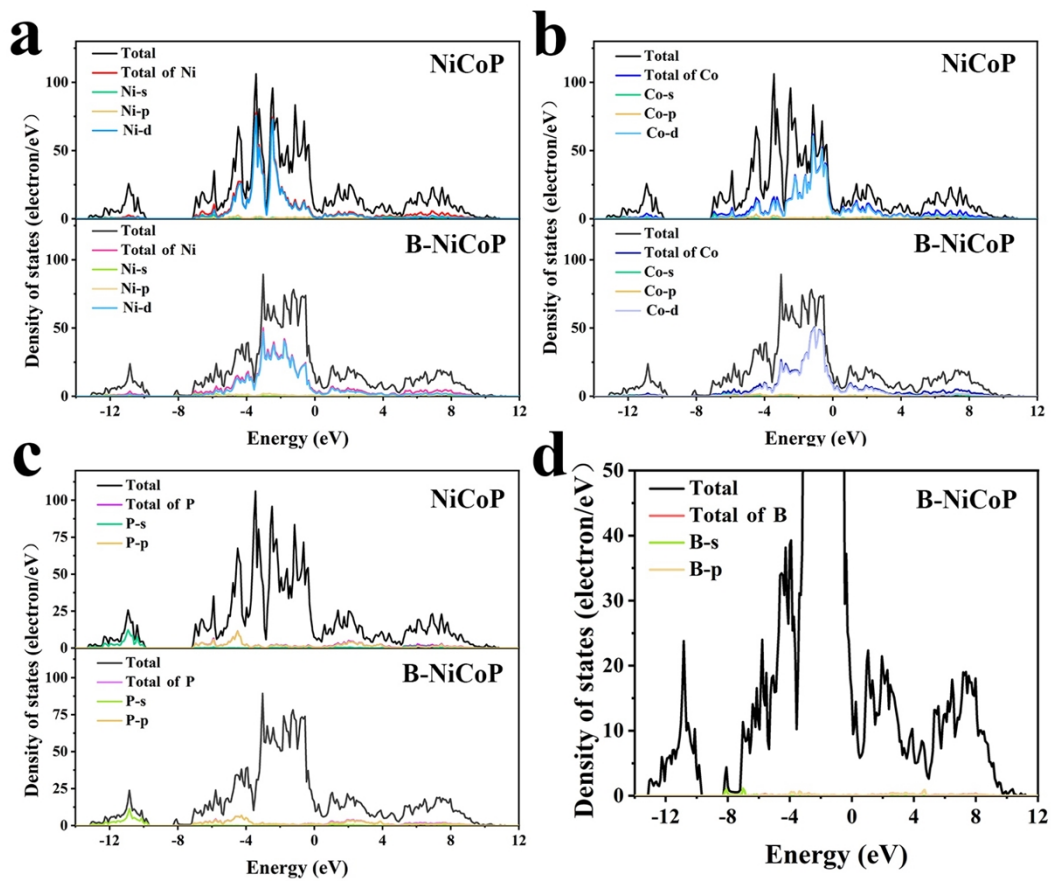
Fig. S8 (a) CV curves and (b) GCD curves of AC
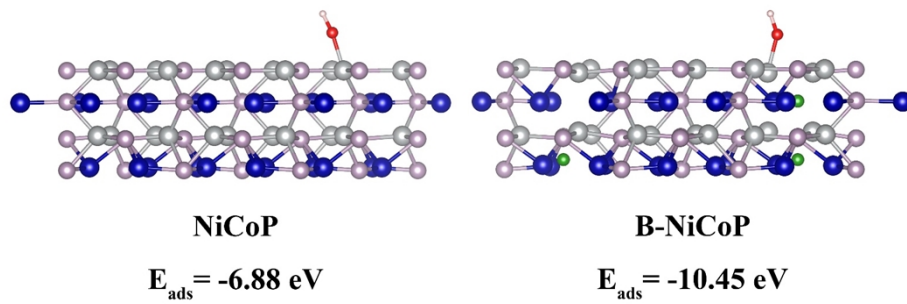
Fig. S9 TDOS and PDOS of (a) Ni, (b) Co, (c) P, and (d) B

NiCoP

E_{ads} = -6.88 eV
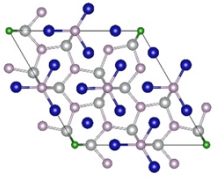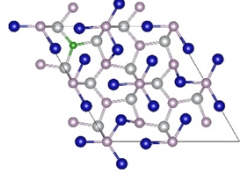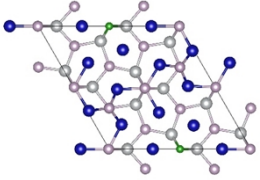
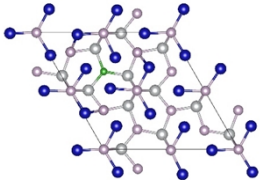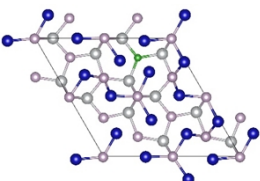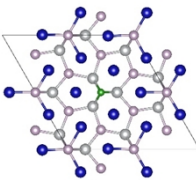**B-NiCoP**

E_{ads} = -10.45 eV
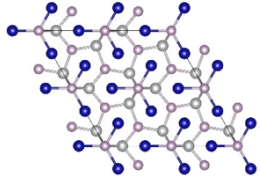
Fig. S10 Optimized adsorption models and adsorption energy of OH⁻ for NiCoP and B-NiCoP

Table S1 Comparison of three electrode properties of B-NCP-CC-18 electrode material with reported positive electrode material

Electrode material	Morphology	Electrolyte	Specific capacity /C g^{-1}	Specific capacity /F g^{-1}	Ref
B-NCP-CC-18	Nanoarrays	3 M KOH	801	1602	This work
Single-Ligand-NiCoP/NC	hollow structure	6 M KOH		1551	1
NiCoP/NPC	folded and hollow spherical structure	3 M KOH	660.3		2
NiCoP/HKUST-1@CNTs	Polyhedral structure	6 M KOH		1154	3
1D NiCoP@C(Zn) nano-cuboids	Hollow nano-cuboids with abundant micropores	6 M KOH		1203	4
Ni1Co1-10P	nanometer tremella flower	6 M KOH		1188.4	5
hollow NiCoP	hollow nanocubes	6 M KOH		1590	6

Table S2 Comparison of d-band centers of Ni and Co when B-doped with different positions of the P-site in NiCoP

Number	D-band center	Model of B-NiCoP
NiCoP	-1.61	
B-NiCoP-1	-1.365	
B-NiCoP-2	-1.409	
B-NiCoP-3	-1.346	
B-NiCoP-4	-1.417	
B-NiCoP-5	-1.416	
B-NiCoP-6	-1.362	

References

1. Z. Cui, F. Yi, T. Meng, A. Gao, J. Hao, Y. Wang, S. Li, J. Huang and D. Shu, Sustainable Mater. Techno., 2023, 37, e00678.
2. M. Yi, B. Lu, X. Zhang, Y. Tan, Z. Zhu, Z. Pan and J. Zhang, Appl. Catal., B, 2021, 283, 119635.
3. R. Zheng, H. Lin, J. Ding, P. Zhou, Y. Ying and Y. Liu, J. Energy Storage, 2024, 75, 109565.
4. G. Wang, A. Gao, T. Zhao, T. Meng, F. Yi, C. Liu, J. Ling, C. He and D. Shu, Chem. Eng. J., 2023, 469, 143852.
5. H. Zhang, H. Guo, J. Zhang, C. Li, Y. Chen, N. Wu, Z. Pan and W. Yang, J. Energy Storage, 2022, 54, 105356.
6. M. Wang, J. Zhong, Z. Zhu, A. Gao, F. Yi, J. Ling, J. Hao and D. Shu, J. Alloys Compd., 2022, 893, 162344.